Special Issue

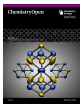

Metal Assisted Synthesis of Cationic Sulfidobismuth Cubanes in Ionic Liquids

Maximilian Knies,[a] Matthias F. Groh,[b] Tobias Pietsch,[a] Mai Lê Anh,[a] and Michael Ruck*[a, c]

Bi_2S_3 was dissolved in the presence of either $AuCl/PtCl_2$ or AgCl in the ionic liquids $[BMIm]Cl \cdot xAlCl_3$ (BMIm = 1-*n*-butyl-3-methylimidazolium; $x = 4$–4.3) through annealing the mixtures at 180 or 200 °C. Upon cooling to room temperature, orange, air-sensitive crystals of $[BMIm](Bi_4S_4)[AlCl_4]_5$ (**1**) or $Ag(Bi_7S_8)[S(AlCl_3)_3]_2[AlCl_4]_2$ (**2**) precipitated, respectively. **1** did not form in the absence of $AuCl/PtCl_2$, suggesting an essential role of the metal cations. X-ray diffraction on single-crystals of **1** revealed a monoclinic crystal structure that contains $(Bi_4S_4)^{4+}$ heterocubanes and $[AlCl_4]^-$ tetrahedra as well as $[BMIm]^+$ cations. The intercalation of the ionic liquid was confirmed via solid state NMR spectroscopy, revealing unusual coupling behavior. The crystal structure of **2** consists of $(Bi_7S_8)^{5+}$ *spiro*-dicubanes, $[S(AlCl_3)_3]^{2-}$ tetrahedra triples, isolated $[AlCl_4]^-$ tetrahedra, and heavily disordered silver(I) cations. No cation ordering took place in **2** upon slow cooling to 100 K.

1. Introduction

Ionic liquids (ILs)[1] are gaining progressively more attention as solvents in inorganic synthesis as they provide access to materials at low temperatures and in high purity or to new compounds that are inaccessible by conventional synthesis methods.[2–6] Beyond their classification as solvents, ILs can also participate in reactions. It can be the weakly coordinating anionic component of the IL, which is incorporated in the resulting product to stabilize complex cationic units,[7] but also the IL cation that acts either as counter ion for complex anions[8–10] or is intercalated into a layered compound.[11–13] In the latter case, the intercalation opened new modification routes, e.g. exfoliation of TiS_2 through swelling of the interlayer spaces or led to the improvement of electrochemical properties of the starting materials, e.g. the catalytic activity of MoS_2[12] or the electrical conductivity in non-aqueous MXenes[14] while upholding high cycling stability.[13] This stimulated the research on the intercalation of IL cations into clays and other materials with the aim to improve adsorption capacities and electrochemical properties.[15–30]

Bismuth(III) sulfide, Bi_2S_3, also known as the mineral bismuthinite, is a hard to dissolve compound, only being soluble under harsh conditions e.g. in hot nitric acid. We recently demonstrated that specific ILs readily dissolve Bi_2S_3 at moderate temperatures.[31,32] This opened a path to compounds that contain either five-atomic Bi_2S_3 molecules $M_2(Bi_2S_3)[AlCl_4]_2$ (M = Cu, Ag)[31] or sulfidobismuth(III) polycations, such as $(Bi_3S_4AlCl)^{3+}$ in $(Bi_3S_4AlCl)[S(AlCl_3)_3][AlCl_4]$[32] or $(Bi_3S_4GaS)^{2+}$ in $(Bi_3S_4GaS)_2[Ga_3Cl_{10}]_2[GaCl_4]_2 \cdot S_8$.[33] However, the first binary sulfidobismuth(III) polycation, the cube-shaped $(Bi_4S_4)^{4+}$ in $(Bi_4S_4)[AlCl_4]_4$, was crystallized from a $NaAlCl_4$ flux by *Beck* et al.[34] Still, the number of sulfidobismuth polycations is small compared to the rich variety of heteroatomic polycations composed of other bismuth-chalcogen or antimony-chalcogen combinations. Those range from isolated heterocubanes $(Bi_4Ch_4)^{4+}$ (Ch = Se, Te)[34,35] over oligo-cubanes to complex *catena* polycations.[36–41]

Herein, we report on the IL-based syntheses and crystal structures of the two new sulfidobismuth(III) compounds $[BMIm](Bi_4S_4)[AlCl_4]_5$ (**1**) and $Ag(Bi_7S_8)[S(AlCl_3)_3]_2[AlCl_4]_2$ (**2**).

2. Results and Discussion

2.1. Syntheses

A mixture of Bi_2S_3 and AuCl or $PtCl_2$, dissolved readily in the ionic liquid $[BMIm]Cl \cdot 4AlCl_3$ (BMIm = 1-*n*-butyl-3-methylimidazolium) at 180 °C. Upon cooling to room temperature, bright orange, air-sensitive crystals of $[BMIm](Bi_4S_4)[AlCl_4]_5$ (**1**) formed, together with $AlCl_3$ and traces of the reduced noble metal. When exposed to moist air, the crystals slowly decompose and release the characteristic odor of H_2S. The assumed mechanism for the decomposition is the hydrolysis of the $[AlCl_4]^-$ ions, resulting in hydrochloric acid, which in turn protonates the sulfide anions to H_2S. The molar ratio of Bi_2S_3 to

[a] M. Knies, T. Pietsch, M. Lê Anh, Prof. Dr. M. Ruck
Faculty of Chemistry and Food Chemistry
Technische Universität Dresden
01069 Dresden (Germany)
E-mail: michael.ruck@tu-dresden.de
Homepage: http://chm.tu-dresden.de/ac2/
[b] Dr. M. F. Groh
Institut für Anorganische Chemie
RWTH Aachen
Landoltweg 1, 52074 Aachen (Germany)
[c] Prof. Dr. M. Ruck
Max Planck Institute for Chemical Physics of Solids
Nöthnitzer Str. 40
01187 Dresden (Germany)

Supporting information for this article is available on the WWW under https://doi.org/10.1002/open.202000246

Special Issue *An invited contribution to a Special Issue dedicated to Material Synthesis in Ionic Liquids*

the metal chlorides was varied from 4:1 to 1:2 (AuCl) and 6:1 to 1:1 ($PtCl_2$). The compound formed in every mixture, but smaller amounts of the metal chloride reduced yield and crystallinity, with only microcrystalline powders found for the lowest concentrations. Although no noble metal was incorporated into the product, as was confirmed by EDS analysis and the crystal structure determination, it seems to be indispensable for the formation of the compound. Synthesis attempts without a metal salt did not lead to the formation of **1**. Similar structure direction through metal cations was previously observed in the synthesis of complex group 14 chalcogenide compounds.[42] PXRD measurements revealed that the metal cations are reduced to elemental gold or platinum (Figure S1 of the Supporting Information). The corresponding oxidation products could not be identified, in particular because of the remaining $AlCl_3$.

In a second synthesis, a mixture of AgCl and Bi_2S_3 in the molar ratio of 2:1 was dissolved in the ionic liquid [BMIm]Cl·4.3$AlCl_3$ at 200 °C. Upon cooling to room temperature, deep red, shiny crystals of $Ag(Bi_7S_8)[S(AlCl_3)_3]_2[AlCl_4]_2$ (**2**) crystallized besides $AlCl_3$ (Figure S2). EDS analyses confirmed the composition, particularly the presence of silver in **2**.

The product formation in this ionothermal synthesis is highly sensitive to the concentrations in the reaction mixture. We used basically the same absolute amounts of AgCl, Bi_2S_3, $AlCl_3$, and [BMIm]Cl as well as the same experimental setup as in a previous report.[31] There $Ag_2(Bi_2S_3)[AlCl_4]_2$ had been obtained as a byproduct, while the main product could not be determined at that time, but was now identified as the silver-poorer $Ag(Bi_7S_8)[S(AlCl_3)_3]_2[AlCl_4]_2$ (**2**). We now observed the formation of $Ag_2(Bi_2S_3)[AlCl_4]_2$ only if the amount of AgCl or the overall concentration of the starting materials in the ionic liquid was increased. Moreover, any attempt to lower the AgCl content to the stoichiometric ratio of **2** resulted in the formation of yellow platelets of a third compound, $[Bi_3S_4AlCl][S(AlCl_3)_3][AlCl_4]$. The latter contains no silver at all and is also accessible by dissolution of Bi_2S_3 in [BMIm]Cl·$x$$AlCl_3$ (x = 3.6; 7.2).[32] Obviously, the chemically available silver(I) is the primary parameter that controls the selectivity. Since AgCl is highly soluble in the used IL and is known to form $[Ag(AlCl_4)Cl]^-$ anions,[43] complexation equilibria seem to be important. A hypothesis, in line with the experimental observations, is that in these $AlCl_3$-rich melts also $[Ag(AlCl_4)_2]^-$ anions form, which mask the silver cations. Such homoleptic tetrachloridoaluminate complexes of silver(I) or copper(I) ions were mentioned in previous electrochemical studies.[44,45] The ratio of the different silver complexes depend on the concentrations and the temperature.

2.2. Crystal Structure of $[BMIm](Bi_4S_4)[AlCl_4]_5$ (1)

1-*n*-butyl-3-methylimidazolium-sulfidobismuth(III)cubane-pentakis[tetrachloridoaluminate(III)], **1**, crystallizes in the monoclinic space group $P2_1/c$ (no. 14) with four formula units per unit cell and the lattice parameters a = 1168.6(1) pm, b = 1786.4(1) pm, c = 2218.0(1) pm, and β = 97.94(1)° at 100(2) K. Atomic parameters and interatomic distances are listed in Tables S1 and S2 of the Supporting Information. The crystal structure (Figure 1) is build up by three different complex ions, $(Bi_4S_4)^{4+}$ heterocubane cations, $[BMIm]^+$ cations, and $[AlCl_4]^-$ tetrahedra. **1** can be regarded a double-salt consisting of *Beck's* $(Bi_4S_4)[AlCl_4]_4$ and the IL [BMIm][$AlCl_4$].

The $(Bi_4S_4)^{4+}$ cation is a distorted cube with bismuth(III) and sulfur(–II) atoms occupying alternating vertices. The Bi–S bond lengths range from 261.8(2) pm to 271.9(2) pm, while the angles within the faces vary between 82.4(1)° and 97.7(1)°, displaying a significant distortion from O_h symmetry. These values span a wider range compared to previous characterizations of this group in $(Bi_4S_4)[AlCl_4]_4$ with Bi–S distances from 263.7(3) pm to 269.7(3) pm and angles from 84.2(1)° to 95.7(1)°.[34] The deviation can partially be attributed to the lower overall symmetry of the monoclinic structure of **1** compared to the tetragonal compound discovered by *Beck*. In both cases, the bond lengths deviate from the distance of 264.8 pm found in the bipyramidal molecular Bi_2S_3 units in $M_2(Bi_2S_3)[AlCl_4]_2$[31] by 7 pm at most.

Taking the surrounding $[AlCl_4]^-$ ions into consideration, each bismuth atom in $(Bi_4S_4)[AlCl_4]_4$ shows a distorted octahedral coordination with Bi–Cl distances between 297.0(2) pm and 310.0(2) pm (Figure 2a).[34] In **1**, the shortest Bi–Cl distance is 294.4(2) pm. Chloride ions at distances of up to 365 pm must be included in the definition of coordination polyhedra to achieve reasonably regular forms. Three of the four independent bismuth positions are surrounded by five chlorine and three sulfur atoms in the shape of a distorted bicapped trigonal prism

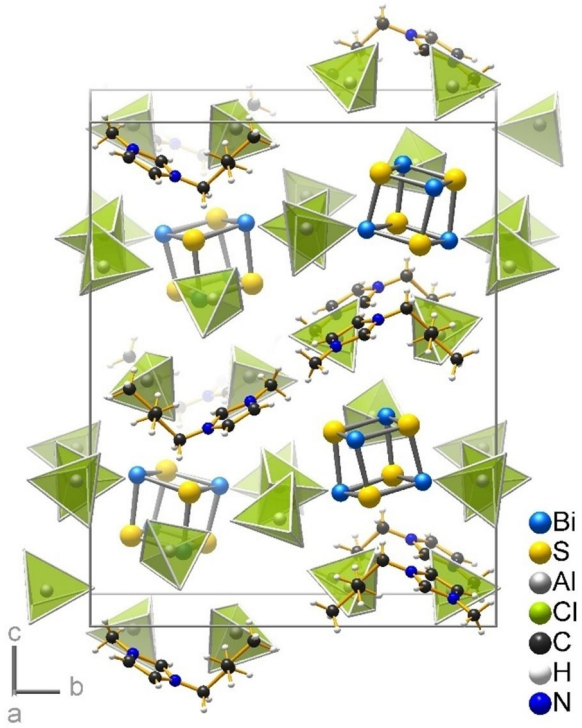

Figure 1. Crystal structure of **1**. The $[BMIm]^+$ fragment is shown with one of the two mutually exclusive positions. $[AlCl_4]^-$ anions are represented as Al-centered polyhedra.

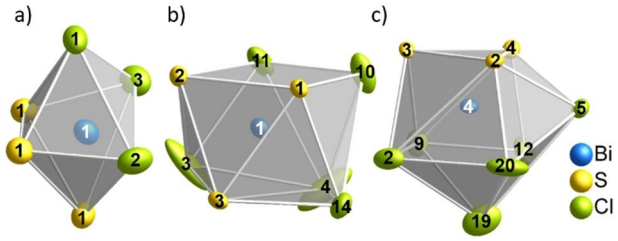

Figure 2. Extended coordination environment of the bismuth atoms in a) $(Bi_4S_4)[AlCl_4]_4$ and in **1** for b) Bi1 and c) Bi4. The ellipsoids comprise 90% probability density of the atoms.

or square antiprism (Figure 2b). The fourth bismuth atom has nine neighbor atoms, which form a distorted tricapped trigonal prism (Figure 2c). In line with the longer Bi–Cl distances, the $[AlCl_4]^-$ ions in **1** are weaker coordinating and show stronger librations than in $(Bi_4S_4)[AlCl_4]_4$.

The organic $[BMIm]^+$ cation is embedded between $[AlCl_4]^-$ groups. It is statistically disordered on two mutually exclusive positions with opposite orientations (Figure 3). Although the two positions are not equivalent, their occupancies appear to be equal. Despite the partial overlap of the two positions, the entire molecules could be identified and refined applying intramolecular distance restraints. The shortest N···Cl distance is

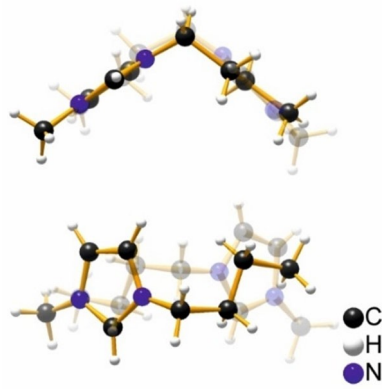

Figure 3. The two mutually exclusive orientations of the $[BMIm]^+$ fragment in the crystal structure of **1**. The 'B' position is shown attenuated.

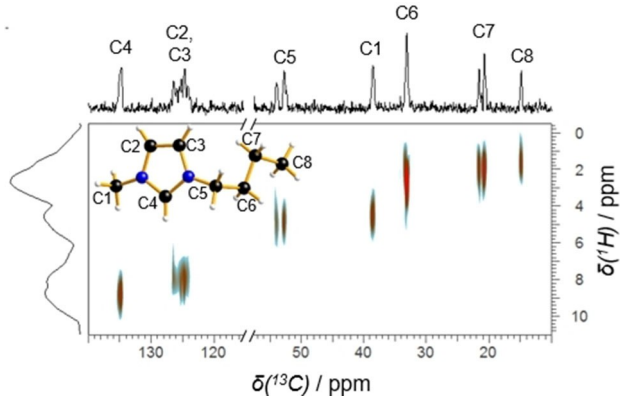

Figure 4. Solid state 2D HETCOR NMR spectrum of $[BMIm](Bi_4S_4)[AlCl_4]_5$.

373 pm and the shortest possible C–H···Cl hydrogen bridges have a C···Cl distance of 340 pm, which indicates only undirected electrostatic interactions between the organic cations and the $[AlCl_4]^-$ anions.

The structure of the embedded $[BMIm]^+$ was confirmed by solid state ^{13}C magic angle spinning (MAS) nuclear magnetic resonance (NMR) spectroscopy (Figure 4). The signals are labeled according to the crystallographic position of the corresponding carbon atom. The chemical shifts are similar to the calculated spectrum of the free $[BMIm]^+$ cation (Figure S3) The differences between both spectra are caused by the chemical environment of the embedded $[BMIm]^+$ molecule. At first glance, a splitting of the resonances of C2, C3, C5 and C7 in the spectrum of **1** is noticeable, which can be attributed to two possible reasons. Because C2, C3 and C5 are each bound to a nitrogen atom, $^{13}C–^{14}N–J$ coupling can occur which can be detected by MAS-NMR. This coupling is unusual for the common liquid state NMR measurement of $[BMIm]^+$ since the second-order quadrupolar effect cannot be transferred from ^{14}N to ^{13}C due to fast relaxation processes. However, in solid state NMR, asymmetric doublets can be observed.[46] Contrary to this, in the ^{13}C-MAS-NMR spectrum of pristine [BMIm]Cl no splitting of these signals could be observed (Figure S3c). Supposedly, the broadening of the signals (FWHM: ca. 50 Hz) prohibits the observation of $^{13}C–^{14}N–J$ coupling. The second reason for differences between calculated and experimental spectra is the presence of $[BMIm]^+$ molecules with different orientations in the crystal structure of **1**. The 2D heteronuclear correlation (HETCOR) spectrum (Figure 4) shows that both signals labeled with C7 in fact have a minor difference in their ^{13}C chemical shift but both show a $^{13}C–^{1}H–J$ coupling with a chemically equivalent hydrogen atom. Hence, the splitting originates from molecules with a different conformation, generating inequivalent C7 positions.[47] This is also indicated in the crystal structure of **1**, in which both orientations show a significantly different C6–C7–C8 bond angle ($\alpha_A = 98(2)°$; $\alpha_B = 116(2)°$). Furthermore, long distance interactions between the $[BMIm]^+$ and $[AlCl_4]^-$ might influence the ^{13}C chemical shift. This is especially the case for C2–C5. Their C–Cl distances are the shortest, but differ greatly between the different orientations of the organic cation ($d_{A(C–Cl)} = 338(1)–348(1)$ pm; $d_{B(C–Cl)} = 364(1)–371(1)$ pm). A similar disorder of the $[BMIm]^+$ cation had been observed in the structure of $[BMIm][Y(Tf_2N)_4]$.[8] Additionally, a general tendency of conformation disorder of the butyl chain has been hinted at in $[BMIm]_2[SnBr_6]$[9] and explored in detail by *Saouane* et al.[10]

2.3. Crystal Structure of $Ag(Bi_7S_8)[S(AlCl_3)_3]_2[AlCl_4]_2$ (2)

Silver(I)-*spiro*[8,8]sulfidobismuth(III)cubane-bis{tris[trichloridoaluminate(III)]sulfide}-bis[tetrachloridoaluminate(III)], **2**, crystallizes in the triclinic space group $P\bar{1}$ (no. 2) with one formula unit per unit cell and the lattice parameters $a = 1064.5(1)$ pm, $b = 1067.0(1)$ pm, $c = 1513.3(1)$ pm, $\alpha = 77.17(1)°$, $\beta = 75.59(1)°$, and $\gamma = 60.42(1)°$ at 298(2) K. Atomic parameters and interatomic distances are listed in Tables S3 and S4 of the Supporting

Information. The crystal structure (Figure 5) features three different complex ions, $(Bi_7S_8)^{5+}$ *spiro*-dicubane cations, $[S(AlCl_3)_3]^{2-}$ anions and $[AlCl_4]^-$ tetrahedra, as well as disordered silver(I) cations.

The structure is organized into layer packages parallel (001) (Figure 6). The layer symmetry is close to the trigonal layer group $p\bar{3}m1$ (no 72).[48] This is also the origin of the almost identical lattice parameters *a* and *b*. The stacking vector of layers includes a shift by $\Delta x \approx 0.25$ and $\Delta y \approx 0.18$. Consequently, the symmetries of neighboring layers do not match, which reduces the total symmetry to the triclinic space group $P\bar{1}$.

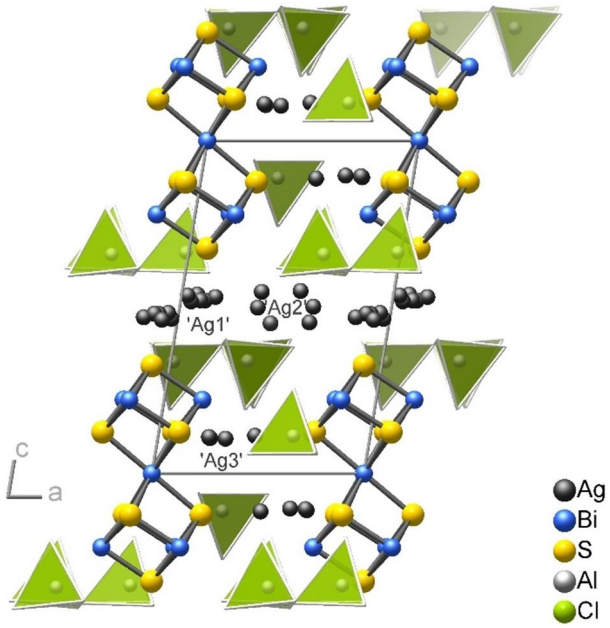

Figure 5. Crystal structure of **2**. $[S(AlCl_3)_3]^{2-}$ and $[AlCl_4]^-$ anions are represented as Al-centered polyhedra.

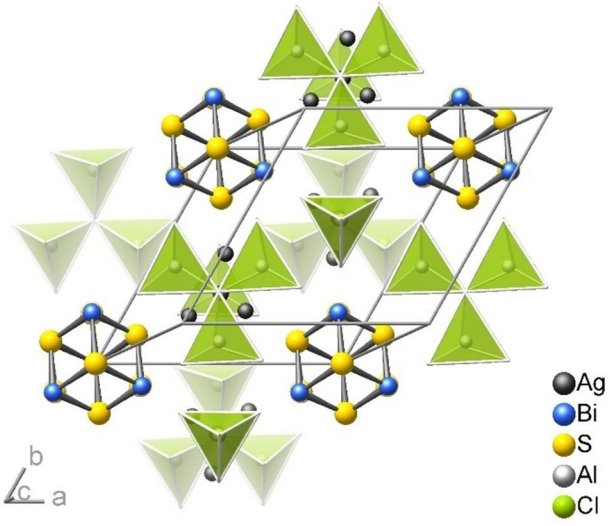

Figure 6. Layer at about $-{}^1/_2 \le z \le {}^1/_2$ in the crystal structure of **2**. The layer symmetry is close to the trigonal layer group $p\bar{3}m1$. The *c*-axis of the unit cell is identical to the stacking vector, which reduces the overall symmetry to the triclinic space group *P*1.

Nonetheless, trigonal pseudosymmetry applies to most parts of the structure.

The hetero *spiro*-dicubane $(Bi_7S_8)^{5+}$ cation (Figure 7) is composed of two $(Bi_4S_4)^{4+}$ cubes that share a common bismuth atom vertex. It is isostructural to $(Sb_7Se_8)^{5+}$ and $(Sb_7Te_8)^{5+}$.[36,37] In accordance with the layer pseudosymmetry, the $(Bi_7S_8)^{5+}$ molecule has the point group symmetry $\bar{3}m$ (D_{3d}) although its crystallographic symmetry is only $\bar{1}$ (C_i). The Bi–S distances range from 259.1(3) pm to 267.2(2) pm for the threefold coordinated bismuth atoms and from 280.9(4) pm to 281.4(3) pm for the central sixfold coordinated bismuth atom. The latter is a rare case of almost regular octahedral coordination of a bismuth(III) atom. Usually, [3 + 3] coordination with clear differentiation into shorter and longer bonds is observed, which in fact is expected to be energetically more favorable for linear three-center bonds. Moreover, the lone-pair of this bismuth(III) atom apparently preserves its spherical 6 s character.[49] The coordination of the outer bismuth atoms is amended by chloride ions to heavily distorted octahedra with Bi–Cl distances ranging from 305.7(3) pm to 330.8(3) pm. These chloride ions belong to both, the $[S(AlCl_3)_3]^{2-}$ and the $[AlCl_4]^-$ groups.

The isolated $[AlCl_4]^-$ tetrahedron is almost regular with one short Al–Cl distance of 210.6(4) pm along the pseudo threefold axis perpendicular to the (001) plane and three quite similar distances ranging from 213.2(4) pm to 213.9(4) pm. These distances are in accordance with those reported for $Na[AlCl_4]$.[50]

The complex anion $[S(AlCl_3)_3]^{2-}$ consist of three $[AlSCl_3]^{2-}$ tetrahedra that share their sulfur atom and point in the same

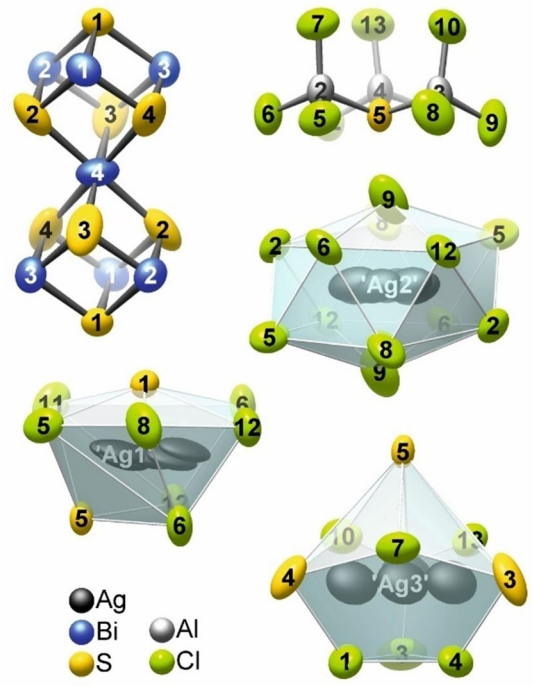

Figure 7. $(Bi_7S_8)^{5+}$ spiro-dicubane cation, $[S(AlCl_3)_3]^{2-}$ anion, and coordination polyhedra of the disordered silver(I) cations in **2**. The ellipsoids comprise 90% of the probability density of the atoms.

direction (Figure 7). The pseudosymmetry is 3 *m* (C_{3v}), while the crystallographic symmetry is only 1 (C_s). The S–Al distances are uniform with lengths between 227.7(3) pm and 228.1(3) pm. This group has first been found in $(Bi_3S_4AlCl)[S(AlCl_3)_3][AlCl_4]$.[32] Most likely, the gallium-centered analog is present in $(Bi_3GaS_5)[Ga_3Cl_{10}]_2[GaCl_4]_2 \cdot S_8$ (taking into account the similar scattering factors of S and Cl).[33]

The silver(I) ions are distributed over at least thirteen partially occupied positions, which form three groups (Figures 5 and 7). 'Ag1' and 'Ag2' are located between the layer packages, while 'Ag3' is in them. The Ag–S distances range from 229(3) pm to 261(4) pm, the Ag–Cl distances from 234(4) pm to 319(3) pm. These ranges were chosen referencing comparable coordination environments in $Ag_2(Bi_2S_3)[AlCl_4]_2$[31] and $Ag[AlCl_4]$.[51]

The group 'Ag1' comprises the majority (56.8%) of the electron density of the silver atom, and is modelled by six individual positions. The surrounding consists of seven chloride and two sulfide ions, which originate from the tip of a $(Bi_7S_8)^{5+}$ polycation as well as four $[S(AlCl_3)_3]^{2-}$ anions. These nine anions form an irregular coordination polyhedron.

The group 'Ag2' includes a center of inversion and consists of two times three individual position, for which the sum of occupancies is 17.1%. Twelve chloride ions form a distorted icosahedron around them. Both complex anions contribute to this coordination polyhedron.

The remaining 26.1% of occupancy are distributed over the four split positions in the group 'Ag3'. The group and its encasing polyhedron show the pseudosymmetry 3 *m* (C_{3v}). The polyhedron is an octahedron of six chloride ions of which four faces are capped by sulfide ions. All building units of the structure contribute to this coordination.

Beck et al. had presented two similar compounds in 2013.[36] $Na(Sb_7Te_8)[MCl_4]_6$ (M = Al, Ga) feature pnicogen-chalcogen *spiro*-dicubane cations surrounded by tetrachloridometalate anions and monovalent cations that show disorder at room temperature. There, the degree of disorder was lower than in **2**, and the cations ordered by cooling the crystals to 123 K. For **2**, the disorder persisted even after a very slow cooling to 100 K. This different behavior might be caused by dissimilar bonding preferences of the soft silver and the hard sodium cations (thermodynamic argument), but also by the bulky $[S(AlCl_3)_3]^{2-}$ group, which does not have the libration modes of isolated tetrahedra (kinetic argument). The sulfide ions seem to partake more in the coordination of the silver ions of **2** compared to telluride and sodium ions in $Na(Sb_7Te_8)[MCl_4]_6$ (M = Al, Ga). Since heavier elements of group 16 are attributed with a better capability to bridge metal centers,[52] this is probably caused by the more covalent nature of interactions between the soft silver and sulfur atoms compared to the hard sodium and soft tellurium atoms.[53]

3. Conclusions

$[BMIm](Bi_4S_4)[AlCl_4]_5$ **1** and $Ag(Bi_7S_8)[S(AlCl_3)_3]_2[AlCl_4]_4$ **2** present two new compounds with pnicogen-chalcogen polycations. The structures comprise the heterocubane $(Bi_4S_4)^{4+}$ and the *spiro*-dicubane $(Bi_7S_8)^{5+}$, which are formed by dissolution of Bi_2S_3 in the IL $[BMIm]Cl \cdot xAlCl_3$ (x = 4–4.3) at moderate temperatures. **1** can be interpreted as a double-salt of $(Bi_4S_4)[AlCl_4]_4$ and the IL $[BMIm][AlCl_4]$. So far, the incorporation of both components of the IL into an inorganic compound has mostly been reported for clay-like materials. Moreover, auxiliary metal chlorides proved necessary for the crystallization of **1**. Similarly, **2** represents an example how product selectivity in ionothermal syntheses can be influenced by small changes of reaction parameters.

Experimental Section

Synthesis

All compounds were handled in an argon-filled glove box (MBraun; $p(O_2)/p^0 < 1$ ppm, $p(H_2O)/p^0 < 1$ ppm). The reactions were carried out in silica ampoules with a length of 120 mm and a diameter of 14 mm. $[BMIm](Bi_4S_4)[AlCl_4]_5$ **1** was synthesized in the ionic liquid $[BMIm]Cl \cdot 4AlCl_3$, which acted as solvent and reactant. The ampoule was loaded with 93.5/40.0/10.0 mg AuCl (99.995%, abcr) or 53.0/9.2 mg $PtCl_2$ (73.27% Pt, Alfa Aesar) respectively, 102.8 mg Bi_2S_3 (99.9%, Alfa Aesar), 150.0 mg [BMIm]Cl (98%, Sigma Aldrich, dried under vacuum at 100 °C), and 450.0 mg $AlCl_3$ (sublimed three times). The evacuated and sealed ampoule was heated at 180 °C for 48 h. The ionic liquid turned black at the reaction temperature. Before cooling the mixture to room temperature at $\Delta T/t = -6$ K/h^{-1}, the ampoule was tilted to enable to separation of already precipitated by-products. Orange crystals of **1** were obtained in sizes from approximately 50 to 1000 μm alongside red $Bi_5[AlCl_4]_3$ and colorless $AlCl_3$. The samples of **1** were washed with dry dichloromethane under inert atmosphere three times. $Ag(Bi_7S_8)[S(AlCl_3)_3]_2[AlCl_4]_2$ **2** was synthesized in the ionic liquid $[BMIm]Cl \cdot 4.3AlCl_3$, which acted as solvent and reactant. The ampoule was loaded with 55.1 mg AgCl (99.98%, Alfa Aesar), 98.6 mg Bi_2S_3 (99.9%, Alfa Aesar), 90.0 mg [BMIm]Cl (98%, Sigma Aldrich, dried under vacuum at 100 °C), and 300.0 mg $AlCl_3$ (sublimed three times). The evacuated and sealed ampoule was heated at 200 °C for 6 d and subsequently tilted and cooled to room temperature at $\Delta T/t = -6$ K/h^{-1}. The IL was decanted from the precipitated colorless $AlCl_3$ and deep red crystals of **2**, which were obtained in sizes of 0.1 to 2 mm. The excess silver(I) ions were not detected in any precipitate and are assumed to remain dissolved in the IL.

EDS Analysis

EDS measurements were conducted using a SU8020 (Hitachi) SEM equipped with a Silicon Drift Detector (SDD) X-Max^N (Oxford) to check the chemical composition of the crystals. However, several problems impeded the interpretation of the measured data. The $[AlCl_4]^-$ ions partially decompose in the high-energetic electron beam (U_a = 20 kV) that is necessary to activate bismuth for this measurement.[54] The preparation had to take place on a carbon pad, which prevented the determination of carbon as well as nitrogen contents. Considering these factors, we were able to support the composition of both compounds regarding the presence or absence of all elements. Calcd./exp. Bi:S:Al:Cl (at.–%) in $[BMIm](Bi_4S_4)[AlCl_4]_5$: 12.1:12.1:15.2:60.6/15.6(8):17.1(8):19(2):48(3). Calcd./exp. Ag:Bi:S:Al:Cl (at.–%) in $Ag(Bi_7S_8)[S(AlCl_3)_3]_2[AlCl_4]_2$: 1.9:13.5:19.2:15.4:50/1.6(3):17(3):16(3):19.3(8):46(5).

Powder X-Ray Diffraction

Data collection was performed at 296(3)K with an X'Pert Pro MPD diffractometer (PANalytical) equipped with a Ge(220) hybrid-monochromator using Cu-$K_{\alpha 1}$ radiation ($\lambda = 154.056$ pm). Due to their sensitivity to moisture, the samples were contained in a glass capillary (Hilgenberg) with an outer diameter of 0.3 mm.

X-Ray Crystal Structure Determination

Single-crystal X-ray diffraction was measured on a four-circle Kappa APEX II CCD diffractometer (Bruker) with a graphite(002)-monochromator and a CCD-detector at $T = 100(2)$ K for **1** and $T = 298(2)$ K for **2**. Mo-K_α radiation ($\lambda = 71.073$ pm) was used. The datasets were corrected for background, polarization and Lorentz factor through the APEX3 software suite.[55] A multi-scan absorption correction using SADABS was applied,[56] and the initial structure solution was performed through a dual-space approach in SHELXT.[57] The structure was refined in SHELXL against F_o^2.[58,59]

$[BMIm](Bi_4S_4)[AlCl_4]_5$: monoclinic; space group $P2_1/c$ (no. 14);

$T = 100(2)$ K; $a = 1168.6(1)$ pm, $b = 1786.4(1)$ pm, $c = 2218.0(1)$ pm, $\beta = 97.94(1)°$; $V = 4586.1(3) \times 10^6$ pm^3; $Z = 4$; $\rho_{calcd.} = 2.746$ g cm^{-3}; μ(Mo–K_α) = 16.8 mm^{-1}; $2\Theta_{max} = 55.7°$, $-15 \le h \le 15$, $-23 \le k \le 23$, $-29 \le l \le 29$; 98333 measured, 10922 unique reflections, $R_{int} = 0.064$, $R_\sigma = 0.037$; 343 parameters, R_1[9057 $F_o > 4\sigma(F_o)$] = 0.028, wR_2(all F_o^2) = 0.056, *GooF* = 1.035, min./max. residual electron density: −1.27/1.66 e × 10^{-6} pm^{-3}.

Two independent, partially overlapping orientations of the $[BMIm]^+$ cation were identified and refined, using distance restraints for the *n*-butyl chain and coupled displacement parameters for all atoms in the molecules. The occupancies refined to 50 % within one standard deviation and were subsequently fixed to this value. For atomic parameters see Table S2 of the Supporting Information.

$Ag(Bi_7S_8)[S(AlCl_3)_3]_2[AlCl_4]_2$: triclinic; space group $P\bar{1}$ (no. 2); T = 298(2) K; $a = 1064.5(1)$ pm, $b = 1067.0(1)$ pm, $c = 1513.3(1)$ pm, $\alpha = 77.17(1)°$, $\beta = 75.59(1)°$, $\gamma = 60.42(1)°$; $V = 1437.7(2) \times 10^6$ pm^3; $Z = 1$; $\rho_{calcd.} = 3.498$ g cm^{-3}; μ(Mo-K_α) = 23.4 mm^{-1}; $2\theta_{max} = 53.1°$, $-13 \le h \le 12$, $-13 \le k \le 13$, $-19 \le l \le 17$; 17640 measured, 5828 unique reflections, $R_{int} = 0.059$, $R_\sigma = 0.053$; 302 parameters, R_1[4545 $F_o > 4\sigma(F_o)$] = 0.042, wR_2(all F_o^2) = 0.095, *GooF* = 1.145, min./max. residual electron density: −1.87/2.54 e × 10^{-6} pm^{-3}. The sum of occupancies for all silver positions was restrained to one Ag per formula unit. The silver atoms were group-wise constrained to have the same anisotropic displacement parameters. For atomic parameters see Table S4 of the Supporting Information.

Further details of the crystal structure determination are available from the Fachinformationszentrum Karlsruhe, D-76344 Eggenstein-Leopoldshafen (Germany), E-mail: crysdata@fiz-karlsruhe.de, on quoting the depository numbers CSD-2017530 for $[BMIm](Bi_4S_4)[AlCl_4]_5$ and CSD-2017529 for $Ag(Bi_7S_8)[S(AlCl_3)_3]_2[AlCl_4]_2$.

Nuclear Magnetic Resonance NMR Spectroscopy

For solid-state NMR experiments a Bruker Avance Neo 300 MHz spectrometer with a 2.5 mm magic angle spinning (MAS) probe was used. The samples were packed in 2.5 mm zirconium oxide rotors with vespel caps in the glove box under argon atmosphere. Cross polarisation (CP) from ^{1}H was used for the ^{13}C measurements. 45,000 scans were recorded with a recycling delay of 3 s at transmitter frequency of 75.47 MHz and a contact time of 3500 µs. 2D – heteronuclear correlation (HETCOR) sequences used 1000 scans times 256 increments and a contact pulse of 200 µs, according to TMS with external standard adamantane (δ_{CH} = 29.5ppm) with a spinning frequency of 15 kHz.

Acknowledgements

This work was financially supported by the Deutsche Forschungsgemeinschaft (DFG) within the priority program SPP 1708. We acknowledge technical support by A. Brünner, P. Kossatz, N. Metzkow and *M. Münch* (all TU Dresden). Open access funding enabled and organized by Projekt DEAL.

Conflict of Interest

The authors declare no conflict of interest.

Keywords: bismuth · heterocubanes · ionic liquids · ionothermal synthesis · spirocubanes

[1] P. Wasserscheid, T. Welton, *Ionic Liquids in Synthesis*, Wiley, **2008**.
[2] D. Freudenmann, S. Wolf, M. Wolff, C. Feldmann, *Angew. Chem. Int. Ed.* **2011**, *50*, 11050–11060; *Angew. Chem.* **2011**, *123*, 11244–11255.
[3] X. Duan, J. Ma, J. Lian, W. Zheng, *CrystEngComm* **2014**, *16*, 2550–2559.
[4] X. Kang, X. Sun, B. Han, *Adv. Mater.* **2016**, *28*, 1011–1030.
[5] Z. Ma, J. Yu, S. Dai, *Adv. Mater.* **2010**, *22*, 261–285.
[6] S. Santner, J. Heine, S. Dehnen, *Angew. Chem. Int. Ed.* **2016**, *55*, 876–893; *Angew. Chem.* **2016**, *128*, 886–904.
[7] M. F. Groh, A. Wolff, M. A. Grasser, M. Ruck, *Int. J. Mol. Sci.* **2016**, *17*, 1452.
[8] A. Babai, A.-V. Mudring, *Z. Anorg. Allg. Chem.* **2008**, *634*, 938–940.
[9] A. Eich, R. Köppe, P. W. Roesky, C. Feldmann, *Eur. J. Inorg. Chem.* **2019**, *2019*, 1292–1298.
[10] S. Saouane, S. E. Norman, C. Hardacre, F. P. A. Fabbiani, *Chem. Sci.* **2013**, *4*, 1270–1280.
[11] T. E. Sutto, T. T. Duncan, *Electrochim. Acta* **2012**, *77*, 204–211.
[12] H. R. Inta, T. Biswas, S. Ghosh, R. Kumar, S. K. Jana, V. Mahalingam, *ChemNanoMat* **2020**, *6*, 685–695.
[13] S. Zheng, C. Zhang, F. Zhou, Y. Dong, X. Shi, V. Nicolosi, Z.-S. Wu, X. Bao, *J. Mater. Chem. A* **2019**, *7*, 9478–9485.
[14] M. Naguib, V. N. Mochalin, M. W. Barsoum, Y. Gogotsi, *Adv. Mater.* **2014**, *26*, 992–1005.
[15] S. Letaief, T. A. Elbokl, C. Detellier, *J. Colloid Interface Sci.* **2006**, *302*, 254–258.
[16] L. Wu, L. Liao, G. Lv, F. Qin, Z. Li, *Chem. Eng. J.* **2014**, *236*, 306–313.
[17] G. K. Dedzo, C. Detellier, *Appl. Clay Sci.* **2014**, *97–98*, 153–159.
[18] C. Takahashi, T. Shirai, M. Fuji, *Mater. Chem. Phys.* **2012**, *135*, 681–686.
[19] T. E. Sutto, P. C. Trulove, H. C. D. Long, *Electrochem. Solid-State Lett.* **2003**, *6*, A50.
[20] C. Aftafa, F. O. Pelit, E. E. Yalçinkaya, H. Turkmen, İ. Kapdan, F. Nil Ertaş, *J. Chromatogr. A* **2014**, *1361*, 43–52.
[21] C. Takahashi, T. Shirai, Y. Hayashi, M. Fuji, *Solid State Ion.* **2013**, *241*, 53–61.
[22] X. Liu, J. Guo, J. Chen, J. Zhang, J. Zhang, *J. Power Sources* **2017**, *363*, 54–60.
[23] W. Wu, J. Wang, J. Liu, P. Chen, H. Zhang, J. Huang, *Int. J. Hydrogen Energy* **2017**, *42*, 11400–11410.
[24] E. E. Yalçınkaya, F. O. Pelit, İ. Güney, H. Türkmen, *J. Porous Mater.* **2014**, *21*, 1151–1158.
[25] L. Zhang, C. Wang, Z. Yan, X. Wu, Y. Wang, D. Meng, H. Xie, *Appl. Clay Sci.* **2013**, *86*, 106–110.
[26] M. S. Nasser, S. A. Onaizi, I. A. Hussein, M. A. Saad, M. J. Al-Marri, A. Benamor, *Colloids Surf.* **2016**, *507*, 141–151.
[27] H. Hu, J. C. Martin, M. Xiao, C. S. Southworth, Y. Meng, L. Sun, *J. Phys. Chem. C* **2011**, *115*, 5509–5514.

[28] J. A. Fiscal-Ladino, M. Obando-Ceballos, M. Rosero-Moreano, D. F. Montaño, W. Cardona, L. F. Giraldo, P. Richter, *Anal. Chim. Acta* **2017**, *953*, 23–31.
[29] L. Wu, C. Yang, L. Mei, F. Qin, L. Liao, G. Lv, *Appl. Clay Sci.* **2014**, *99*, 266–274.
[30] J. Fan, Q. Xiao, Y. Fang, L. Li, W. Feng, W. Yuan, *ChemElectroChem* **2019**, *6*, 676–683.
[31] M. F. Groh, M. Knies, A. Isaeva, M. Ruck, *Z. Anorg. Allg. Chem.* **2015**, *641*, 279–284.
[32] M. F. Groh, A. Isaeva, U. Müller, P. Gebauer, M. Knies, M. Ruck, *Eur. J. Inorg. Chem.* **2016**, *6*, 880–889.
[33] D. Freudenmann, C. Feldmann, *Dalton Trans.* **2010**, *40*, 452–456.
[34] J. Beck, S. Schlüter, N. Zotov, *Z. Anorg. Allg. Chem.* **2004**, *630*, 2512–2519.
[35] J. Beck, M. Dolg, S. Schlüter, *Angew. Chem.* **2001**, *113*, 2347–2350; *Angew. Chem. Int. Ed.* **2001**, *40*, 2287–2290.
[36] A. Eich, S. Schlüter, G. Schnakenburg, J. Beck, *Z. Anorg. Allg. Chem.* **2013**, *639*, 375–383.
[37] A. Eich, W. Hoffbauer, G. Schnakenburg, T. Bredow, J. Daniels, J. Beck, *Eur. J. Inorg. Chem.* **2014**, *2014*, 3043–3052.
[38] Q. Zhang, I. Chung, J. I. Jang, J. B. Ketterson, M. G. Kanatzidis, *J. Am. Chem. Soc.* **2009**, *131*, 9896–9897.
[39] E. Ahmed, A. Isaeva, A. Fiedler, M. Haft, M. Ruck, *Chem. Eur. J.* **2011**, *17*, 6847–6852.
[40] E. Ahmed, J. Breternitz, M. F. Groh, A. Isaeva, M. Ruck, *Eur. J. Inorg. Chem.* **2014**, *2014*, 3037–3042.
[41] J. Beck, S. Schlüter, *Z. Anorg. Allg. Chem.* **2005**, *631*, 569–574.
[42] S. Santner, A. Wolff, M. Ruck, S. Dehnen, *Chem. Eur. J.* **2018**, *24*, 11899–11903.
[43] X. Pang, Y. Liu, J. Wang, *Catalysts* **2018**, *8*, 498.
[44] T. Sato, M. Ueda, I. Saeki, *Electrochemistry* **2005**, *73*, 736–738.
[45] C. Nanjundiah, R. A. Osteryoung, *J. Electrochem. Soc.* **1983**, *130*, 1312–1318.
[46] R. K. Harris, A. C. Olivieri, *Prog. Nucl. Magn. Reson. Spectrosc.* **1992**, *24*, 435–456.
[47] F. Liu, A. M. Orendt, D. W. Alderman, D. M. Grant, *J. Am. Chem. Soc.* **1997**, *119*, 8981–8984.
[48] V. Kopský, D. B. Litvin, *International Tables for Crystallography. Volume E, Subperiodic Groups*, Kluwer Academic Publishers, London, **2002**.
[49] A. Isaeva, M. Ruck, *Inorg. Chem.* **2020**, *59*, 3437–3451.
[50] E. Perenthaler, H. Schulz, A. Rabenau, *Z. Anorg. Allg. Chem.* **1982**, *491*, 259–265.
[51] M. Knies, M. Lê Anh, U. Keßler, M. Ruck, *Z. Naturforsch. B* **2020**, *75*, 117–123.
[52] M. W. Degroot, J. F. Corrigan, *Compr. Coord. Chem. II*, Pergamon, Oxford, **2003**, pp. 57–123.
[53] R. G. Pearson, *J. Am. Chem. Soc.* **1963**, *85*, 3533–3539.
[54] U. Müller, A. Isaeva, J. Richter, M. Knies, M. Ruck, *Eur. J. Inorg. Chem.* **2016**, *2016*, 3580–3584.
[55] Bruker, *APEX3 Suite for Crystallographic Software*, Bruker AXS Inc., Madison, Wisconsin, USA, **2017**.
[56] G. M. Sheldrick, *SADABS: Area-Detector Absorption Correction*, Bruker AXS Inc., Madison, Wisconsin, USA, **2016**.
[57] G. M. Sheldrick, *Acta Crystallogr. Sect. A* **2015**, *71*, 3–8.
[58] G. M. Sheldrick, *SHELXL, Program for Crystal Structure Refinement – Multi-CPU*, Georg-August-Universität Göttingen, Göttingen, Germany, **2014**.
[59] G. M. Sheldrick, *Acta Crystallogr. Sect. A* **2008**, *64*, 112–122.

Manuscript received: August 27, 2020
Revised manuscript received: September 21, 2020